PEOPLE'S DEMOCRATIC REPUBLIC OF ALGERIA

MINISTRY OF HIGHER EDUCATION AND SCIENTIFIC RESEARCH

NATIONAL POLYTECHNIC SCHOOL

المدرسة الوطنية المتعددة التقنيات
Ecole Nationale Polytechnique

Electronics Department

Electronics Master Dissertation

Topic:

Sensorless speed field oriented control of induction machine

Presented By:

MESSINI Merouane

Dissertation Committee:

Mr. M.S.AIT-CHEIKH	**Professor**	**ENP**	**President**
Mr. M.HADDADI	**Professor**	**ENP**	**Examiner**
Mr. C.LARBES	**Professor**	**ENP**	**Supervisor**

ENP June 2016

Ecole Nationale Polytechnique (ENP)
10, AVENUE des Frères Oudek, Hassen Badi, BP.182, 16200 EL Harrach, Alger, Algérie
www.enp.edu.dz

ملخص

في هذا العمل ،طُور التحكم الشعاعي من أجل فصل التدفق والعزم. كما استعملت المضبطات PI لضبط السرعة والتيار. أُستعملنا ايضا برنامج Matlab/Simulink من أجل المحاكاة لإظهار سير خوارزمية التحكم الشعاعي. هده الاخيرة تم تثبيتهاعلى البطاقة DSPF28335.

كلمات مفتاحية: محرك لا متزامن، مقدر السرعة، التحكم الشعاعي.

RESUME

Dans ce travail, La commande vectorielle a été développée pour découpler le flux et le couple. Des régulateurs PI ont été conçus pour régler la vitesse et le courant. La simulation par Matlab/Simulink a été employée pour montrer le fonctionnement de l'algorithme FOC. L'estimateur de vitesse a été étudié et utilisé dans l'algorithme de la commande vectorielle, ce dernier a été implémenté sur la carte DSP F28335.

Mots clés : Moteur à induction, estimateur de vitesse, Commande vectorielle, DSP.

ABSTRACT

In this work, Field oriented control method was developed to get the decoupled control of flux and torque. PI based controllers were designed for speed and current control loop. The computer simulation Matlab/Simulink was used to show the efficacy of the FOC algorithm. The speed estimator was studied and used in field oriented control algorithm; this last was implemented on DSP F28335.

Key words: Induction motor, Speed estimator, FOC, DSP.

ACKNOWLEDGEMENTS

I wish to express my sincere gratitude to my supervisor Pr C.LARBES, who has been a constant source of guidance, support and encouragement throughout my graduate studies. His extensive knowledge, rigorous research attitude, diligent working and creative thinking have inspired me and will definitely benefit my future career.

Finally I would like to thank my parents for their love and support.

They are the strength behind my success.

DEDICATION

To my parents, my family, my teachers and anyone who ever shared their knowledge with me.

TABLE OF CONTENTS

LIST OF FIGURES

Figure page

LIST OF TABLES

Table page

LIST OF SYMBOLS

EVs	Electric vehicles.
DC	Direct Current.
AC	Alternative Current.
DSP	Digital Signal Processor.
PWM	Pulse Width Modulation.
SVPWM	Space Vector Pulse Width Modulation.
FOC	Field Oriented Control.
VSI	Voltage Source Inverter
DFOC	Direct Field Oriented Control
IFOC	Indirect Field Oriented Control
CCS	Code Composer Studio
ADC	Analog to digital converter
FPU	Floating Point Unit
PLL	Phase Locked Loop
SARAM	Single Access Random Access Memory
ROM	Read Only Memory
OTP	One Time Programmable memory
DMA	Direct Memory Access
QEP	Quadrature Encoder Pulse
PIE	Peripheral Interrupt Expansion
MUX	Multiplexer
SOC	Start Of Conversion

GPIO	General Purpose Input/Output
TI	Texas Instruments
R	Magnetic circuit reluctance.
i_a	Phase a current.
I_b	Phase b current.
i_c	Phase c current.
i_m	Current magnitude.
N_{sync}	Synchronous speed.
f	Frequency.
P	Number of poles.
N_{slip}	Slip speed.
S	Slip.
a_{eff}	Equivalent turns ratio
n_s	Number of turns per stator phase
n_r	Number of turns per rotor phase
v^s_{abc}	Three phase stator voltage
i^s_{abc}	Three phase stator current
λ^s_{abc}	Three phase stator flux
v^r_{abc}	Three phase rotor voltage
i^r_{abc}	Three phase rotor current
λ^r_{abc}	Three phase rotor flux
r_s	Stator resistance
r_r	Rotor resistance

$L_{as,bs,cs}$	Total self inductance of phase as,bs,cs
L_{ls}	Self inductance of stator phase
L_{ms}	Magnetizing inductance of stator phase
$L_{abs,}$ L_{bcs} , L_{cas}	The mutual inductance between stator three phase
θ_r	Angle from the rotor to the stator phase
(a,b,c)	Three coordinate system
(α,β)	Two coordinate stationary frame
(d,q)	Two coordinate rotating frame
θs	Angle of stator magnetic field
T_e	Torque
ω_S	Electrical speed
ω_r	Mechanical speed
P_e	Electric power
T_L	Load torque
J	Rotor's moment of inertia
m	Modulation index
ω	Angular velocity
$T_0, T_1 T_2$	Duty cycles
Van,bn,cn	Phase voltage
Vab,bc,ca	Line to line voltage
S1 to S6	Switching variable vectors
V_0 to V_7	Space voltage vectors
Vdc	DC main bus Voltage

Introduction

The control and estimation of induction motor drives is a vast subject.Traditionally, the induction machine has been used with constant frequency sources and the squirrel-cage machine is currently utilized in many industrial applications, from chemical plants and wind generation to locomotives and electric vehicles. Its main advantages are the mechanical and electrical simplicity and ruggedness, the lack of rotating contacts (brushes) and its capability to produce torque over the entire speed range.

With the development and maturing of the field-oriented or vector control theory that started about three decades ago, researchers have more and more considered the induction machine a good candidate for variable speed and servo applications. The objectives are related to either process control or energy savings.

Generally, control and estimation of induction machine drives is more difficult than that of dc drives. The main reasons are the complex dynamic behavior and the need to execute relatively complicated calculations for estimation and control using microprocessors with limited cost, speed and accuracy.

Recently, sensorless vector control has received a lot of attention. The elimination of the speed sensor reduces the hardware complexity, size, and cost and increases the reliability of the drive. The requirement is to have a high-performance four-quadrant drive that can deliver controllable torque over the entire speed range. While for medium and high speeds the problem has been solved, stable operation and good performance at low speeds has not been robustly achieved.

The objective of this dissertation is to develop improved control and estimation algorithms for the induction machine.

Project outlines

We start with an Introduction.

Chapter1: the theory of filed orientation control for an induction motor and the simulation results using Matlab/Simulink will be introdued in this chapter.

Chapter 2:Speed Estimator is developed and presented in this chapter

Finally a Conclusion.

CHAPTER 1

FIELD ORIENTED CONTROL

1.1 INTRODUCTION

The DC motors have been widely used in variable speed control applications. In DC drives, the torque and flux are decoupled and can be controlled by the armature and field current. However, DC machines have many disadvantages, such as sparks, commutator and brushes wear out, difficulty to maintain, etc. The field oriented control of induction motor was first developed by Hasse in 1969 and Blaschke in 1972. The development in power electronics devices and microprocessors make the AC machines speed control available and overcome the disadvantages of DC machines like high cost, commutator and brushes problems. Initially, the speed control of induction machine is performed by changing the voltage and frequency and keeping the V/f ratio constant. These types of controlling methods are called the scalar control methods. The high performance of field oriented control drives outperforms the scalar control method due to the following advantages [1]:

- Full torque control capability at low speed.
- Better dynamic behavior.
- Higher efficiency.
- Operating point in a wide range of speed.
- Decoupled torque and flux control.
- Four quadrant operation.

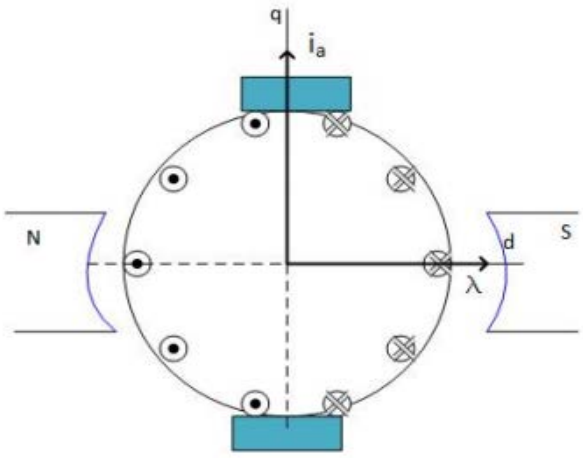

Fig 1.1: A simple representation of DC motor

As we apply the concept of DC motor control to the AC machines, in DC motor the torque is proportional to the cross product of current i_a and flux λ_f. The current and flux are along the two axis of coordinate system, which means they are always perpendicular to each other and produces maximum torque all the time. The torque equation of DC motor which can be used as reference for field oriented control is

$$\tau_m = K_T \lambda_f i_a \qquad (1.1)$$

Where K_T is torque constant.

1.1.1 MODEL OF FIELD ORIENTED CONTROL [2]

The DC machine control approach to AC Drives is not easier, because the orientation of stator and rotor fluxes are not held orthogonal and vary with the operating conditions [1].

To obtain like DC machine control one need to align stator currents with respect to the rotor flux to get independently controlled torque and flux. This type of control is achieved by:

- Converting AC motor dynamics into dq synchronous frame under certain conditions.
- Aligning the flux of the machine to the reference frame.

Depending upon the alignment of flux, the system categorized into two different schemes:

- Stator field oriented control “the reference frame is aligned to the stator field”
- Rotor field oriented control “the reference frame is aligned to the rotor field”

However, calculation of the rotor flux is carried in two different ways. If it is measured directly by using sensors, then it is called direct Field Oriented Control (DFOC).If the measurement is from slip that is calculated from the dynamic model of induction motor, then it is called indirect Field Oriented Control (IFOC). The simplicity of implementation and the more reliability makes IFOC widely used in industries.

In DFOC the rotor flux is measured from Hall Effect sensors. Therefore, the rotor angle can be calculated from the rotor flux by the equation:

$$\theta = tan^{-1} \frac{\lambda_{dr}^{s}}{\lambda_{qr}^{s}} \qquad (1.2)$$

The installation of flux sensors is difficult due to limitations of air gap space, armature reaction, noise, etc. Due to these limitations the rotor flux is calculated indirectly from stator currents that are measured using current sensors.

In IFOC we have two approaches of measuring rotor flux angle. The first one is by calculating the rotor flux equations indirectly by using the stator flux and currents .and the second is from slip information ω_{sl}.

How do we precede with the rotor flux equations from the stator currents and fluxes?

The current sensors are used to measure the stator currents, and fluxes can be obtained using equations (1.3) and (1.4).

$$\lambda_d^s = \int_0^t (v_d^s - r_s i_d^s) dt \tag{1.3}$$

$$\lambda_q^s = \int_0^t (v_q^s - r_s i_q^s) dt \tag{1.4}$$

By converting the equations of the stator flux and rotor flux in synchronous rotating frame into $\alpha\beta$ stationary coordinate frame by multiplying with $e^{j\theta}$, we obtain:

$$\lambda_\alpha^s = L_s i_\alpha^s + L_m i_\alpha^r \tag{1.5}$$

$$\lambda_\beta^s = L_s i_\beta^s + L_m i_\beta^r \tag{1.6}$$

$$\lambda_\alpha^r = L_r i_\alpha^r + L_m i_\alpha^s \tag{1.7}$$

$$\lambda_\beta^r = L_r i_\beta^r + L_m i_\beta^s \tag{1.8}$$

Now we substitute the i_α^r , i_β^r taken from (1.5) and (1.6) in (1.7) and (1.8) we get

$$\lambda_\alpha^r = \frac{L_r(\lambda_\alpha^s + L_s i_\alpha^s)}{L_m} + L_m i_\alpha^s = \frac{(L_m^2 - L_s L_r) i_\alpha^s + L_r \lambda_\alpha^s}{L_m}$$

$$\lambda_\beta^r = \frac{L_r(\lambda_\beta^s + L_s i_\beta^s)}{L_m} + L_m i_\beta^s = \frac{(L_m^2 - L_s L_r) i_\beta^s + L_r \lambda_\beta^s}{L_m}$$

$$\sigma = 1 - \frac{L_m}{L_s L_r} \tag{1.9}$$

After rearranging the terms and substituting terms, the two equations can be written as:

$$\lambda_\alpha^r = \frac{L_r}{L_m}(\lambda_\alpha^s + \sigma L_s i_\alpha^s) \tag{1.10}$$

$$\lambda_\beta^r = \frac{L_r}{L_m}(\lambda_\beta^s + \sigma L_s i_\beta^s) \quad (1.11)$$

Now, substituting the stator currents measured from sensors and fluxes from (1.3) and (1.4) in the above equations, we get rotor flux equations. From (1.10) and (1.11), the rotor flux angle can be obtained. However, this method is not suitable when a DC offset is present.

The second method for calculating rotor flux angle, which is from slip information.

we know that

$$0 = r_r i_d^r + p\lambda_d^r - (\omega - \omega_r)\lambda_q^r$$

$$0 = r_r i_q^r + p\lambda_q^r + (\omega - \omega_r)\lambda_d^r$$

Now applying λ_q^r =0 and $p\lambda_q^r$ = 0, the rotor equations become:

$$0 = r_r i_d^r + p\lambda_d^r \quad (1.12)$$

$$0 = r_r i_q^r + (\omega - \omega_r)\lambda_d^r \quad (1.13)$$

we know λ_d^r and substituting that in (1.12) we get:

$$0 = r_r i_d^r + p(L_r i_d^r + L_m i_d^s)$$

$$0 = (r_r + pL_r) i_d^r + pL_m i_d^s \quad (1.14)$$

$$i_d^r = \frac{-pL_m i_d^s}{(r_r + pL_r)} \quad (1.15)$$

Again by substituting i_d^r in λ_d^r :

$$\lambda_d^r = L_r \frac{-pL_m i_d^s}{(r_r + pL_r)} + L_m i_d^s$$

$$= [L_m - \frac{L_r L_m i_d^s}{(r_r + pL_r)} p] i_d^s$$

After canceling the respective terms the rotor flux along the direct axis, λ_d^r can be written as

$$\lambda_d^r = \frac{L_m}{(1 + pT_r)} i_d^s \quad (1.16)$$

Where T_r is the rotor time constant

$$T_r = \frac{L_r}{r_r} \tag{1.17}$$

In the steady state

$$\lambda_d^r = L_m i_d^s \tag{1.18}$$

Since$\lambda_d^r = 0$, now we can write $i_q^r = -\frac{L_m i_q^s}{L_r}$, substituting this equation in (1.13) we obtain the slip speed information.

Slip_speed = $\omega_{sl} = \omega_s - \omega_r = \frac{r_r}{L_r}\frac{L_m}{\lambda_d^r} i_q^s$ (1.19)

Now, adding obtained slip speed to the rotor shaft speed, we get synchronous speed of the machine. The rotor flux angle can be measured by integrating the synchronous speed which is shown in (1.20)

$$\theta = \int_0^t \omega_e dt = \int_0^t (\omega_{sl} + \omega_r) dt \tag{1.20}$$

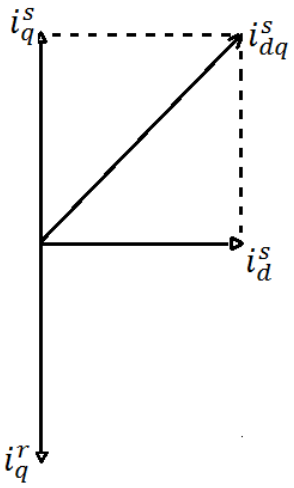

Fig 1.2: The vector representation of rotor field oriented scheme

From $\lambda_d^r = \frac{L_m}{(1+pT_r)} i_d^s$, we find that i_d^s is used to generate rotor flux.

Comparing the equations (1.78) and (3.18), we obtain $i_d^r = 0$.

i_q^s is proportional to the slip.

From $i_q^r = -\frac{L_m i_q^s}{L_r}$, we find i_q^r nullifies flux caused by i_q^s.

The $\lambda_q^r = 0$ reduces the torque equation (1.103) to follow the equation, which is similar to the DC machine

$$T_e = \frac{3}{2}\frac{P}{2}\frac{L_m}{L_r}(\lambda_d^r i_q^s) \qquad (1.21)$$

Based on the field oriented control method, we have the flux along the direct axis and current along the quadrature axis, which is similar to the DC machine. Based on (1.18) and (1.19), the rotor flux along the direct axis is proportional to the i_d^s and the current i_q^s along the quadrature axis is proportional to slip. The two currents i_d^s, i_q^s are used for the control of Induction machine.

1.1.2 FOC ALGORITHM

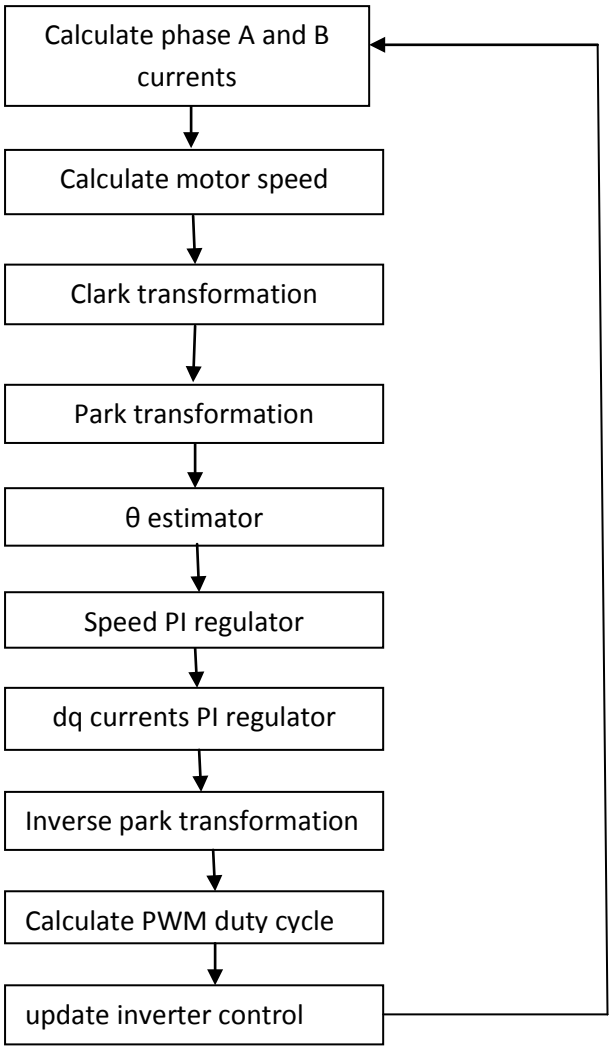

Fig 1.3: The flow chart of the FOC algorithm

The Basic Scheme for Field Oriented Control of Induction Motor

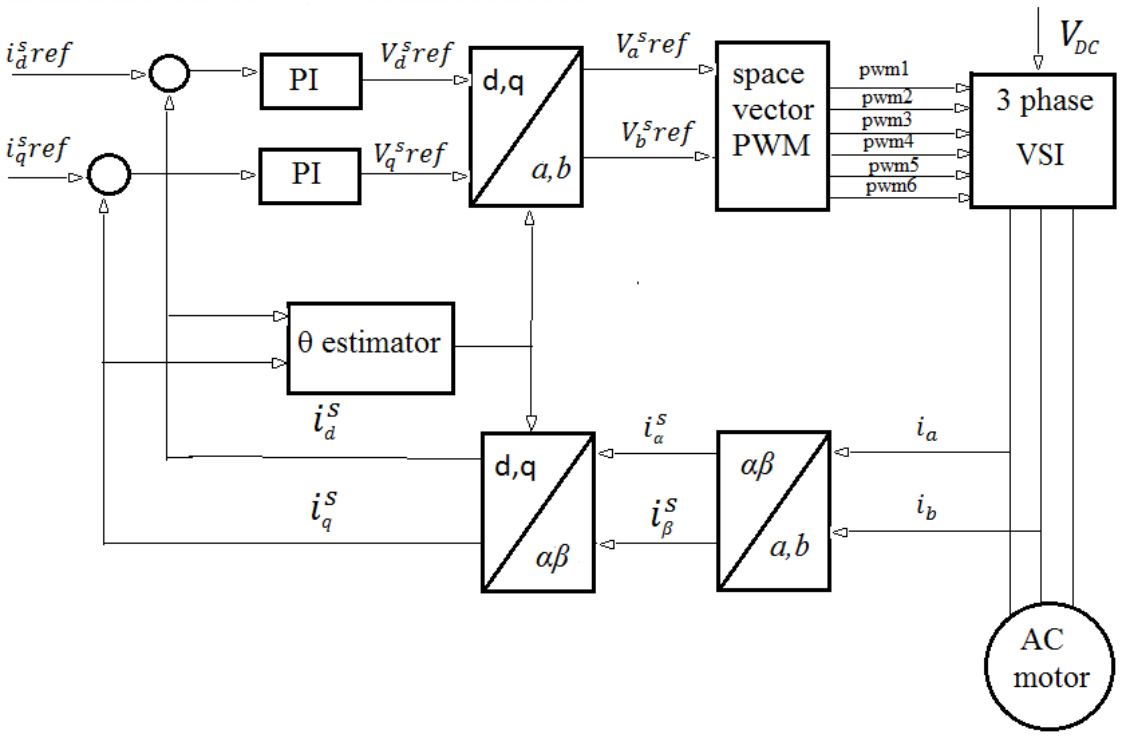

Fig 1.4: The basic scheme of field oriented control

Fig 1.4, explains the basic scheme of speed control with FOC. Firstly, it measures the two input currents of the motor. These input currents are converted to stationary coordinate frame using Clarke's transformation module. The currents in the stationary frame are converted to rotating frame using Park's transformation module. These currents are compared to the reference currents and the resulting error is passed through the current controllers. The output of current controllers, which are in *dq* coordinate frame, are converted into *αβ* coordinate frame using inverse rotating Park's transformation module. These are input to the Space Vector PWM module. The output of Space Vector PWM module operates the gating signal of the three phase inverter. The Clarke and Park Transformation modules require the rotor flux position which is the key factor in controlling the machine. The calculation of rotor flux position is mentioned in direct and indirect rotor field oriented scheme.

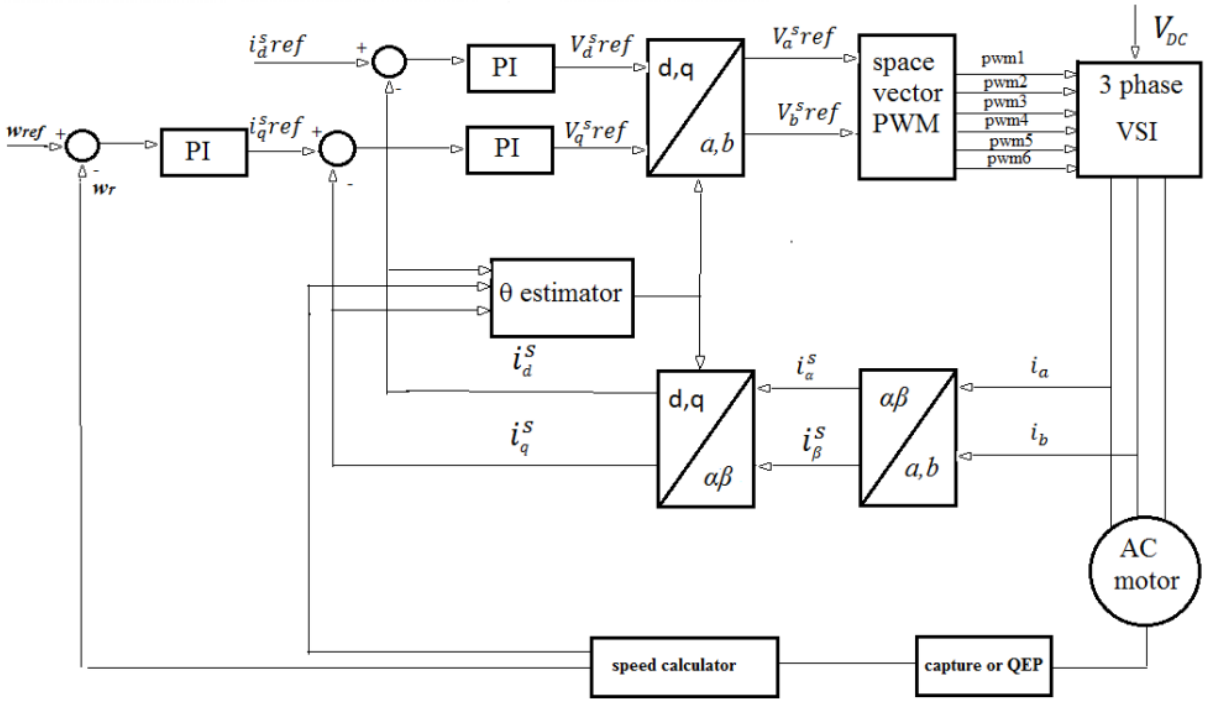

Fig 1.5: Block diagram of indirect rotor field oriented control

1.2 ROTOR FIELD ORIENTED SCHEME

The current can be written as

$$i_d^r = \frac{1}{L_r}(\lambda_d^r - L_m i_d^s) \tag{1.22}$$

$$i_q^r = \frac{1}{L_r}(\lambda_q^r - L_m i_q^s) \tag{1.23}$$

Substituting (1.22) and (1.23) into the system model

$$v_d^s = (r_s + p\sigma L_s)i_d^s + \frac{L_m}{L_r}p\lambda_d^r - \omega\left[\frac{L_m}{L_r}\lambda_q^r + L_s\sigma i_q^s\right] \tag{1.24}$$

$$v_q^s = (r_s + p\sigma L_s)i_q^s + \frac{L_m}{L_r}p\lambda_q^r - \omega\left[\frac{L_m}{L_r}\lambda_d^r + L_s\sigma i_d^s\right] \tag{1.25}$$

Where

$$\sigma = (1 - \frac{L_m}{L_s L_r})$$

The field oriented control can be achieved by aligning the rotor flux along the direct axis, i.e.$\lambda_q^r = 0$, and $p\lambda_q^r = 0$. Therefore, (1.24) and (1.25) are reduced to

$$v_d^s = (r_s + p\sigma L_s)i_d^s + \frac{L_m}{L_r}p\lambda_d^r - \omega_e\left[L_s\sigma i_q^s\right] \quad (1.26)$$

$$v_q^s = (r_s + p\sigma L_s)i_q^s - \omega_e\left[\frac{L_m}{L_r}\lambda_d^r + L_s\sigma i_d^s\right] \quad (1.27)$$

The torque equation became

$$T_e = \frac{3}{2}\frac{P}{2}\frac{L_m}{L_r}(\lambda_d^r i_q^s) \quad (1.28)$$

Applying the Laplace transformation for above two voltage equations and considering the steady state condition $p\lambda_q^r = 0$

$$i_d^s = \frac{\frac{1}{L_s\sigma}}{s+\frac{r_s}{L_s\sigma}}v_d^s + \frac{\omega_e}{s+\frac{r_s}{L_s\sigma}}i_q^s \quad (1.29)$$

$$i_q^s = \frac{\frac{1}{L_s\sigma}}{s+\frac{r_s}{L_s\sigma}}v_q^s - \frac{\omega_e}{s+\frac{r_s}{L_s\sigma}}i_d^s - \frac{\frac{L_m}{L_r L_m\sigma}}{s+\frac{r_s}{L_s\sigma}}\omega_e\lambda_d^r \quad (1.30)$$

Neglecting the r_s term and considering $p\lambda_q^r = 0$ for the steady state condition, we reach the following conditions:

$$L_s\sigma\frac{d}{dt}i_d^s = v_d^s + \omega_e L_s\sigma i_q^s \quad (1.31)$$

$$L_s\sigma\frac{d}{dt}i_q^s = v_q^s - \omega_e L_s\sigma i_d^s - \omega_e\frac{L_m}{L_r}\lambda_d^r \quad (1.32)$$

From (1.26) and (1.27) we find $\omega_e L_s\sigma i_q^s$ and $-\omega_e L_s\sigma i_d^s$, are cross-coupling current terms of d-axis and q-axis. In order to decouple the coupling terms, the feed-forward control is used.

Equate right hand side of equations (1.31) and (1.32) with u_d^* and u_q^*, we have

$$u_d^* = u_d^s + \omega_e L_s\sigma i_q^s \quad (1.33)$$

$$u_q^* = u_q^s - \omega_e L_s\sigma i_q^s - \omega_e\frac{L_m}{L_r}\lambda_d^r \quad (1.34)$$

By applying the Laplace transformation, we have the plant transfer function $G_i(s)$ for the current control as

$$G_i(s) = \frac{i_d^s}{u_d^*} = \frac{1}{L_s \sigma s} \tag{1.35}$$

$$G_i(s) = \frac{i_q^s}{u_q^*} = \frac{1}{L_s \sigma s} \tag{1.36}$$

Where $\sigma = (1 - \frac{L_m}{L_s L_r})$

1.2.1 PI CURRENT CONTROLLER DESIGN

Let's consider the PI controller given below

$$R_i(s) = k_p(1 + \frac{1}{sT_i}) \tag{1.37}$$

Where $T_i = \frac{k_p}{k_i}$

We design the current controller based on frequency response method using the phase and gain margin. Let us choose the crossover frequency, $\omega_c = \frac{2\pi f_s}{10}$, where f_s is the switching frequency of the inverter and phase margin PM = 60^0, i.e.

$$\left|G_{i,o}(j\omega_c)\right| = 1 \tag{1.38}$$

$$\arg\left(G_{i,o}(j\omega_c)\right) = -\frac{2\pi}{3} \tag{1.39}$$

The transfer function of the plant to be controlled is (1.31) for direct and (1.32) for quadrature axis current control respectively. The overall schematic for current control loop is shown in Fig 1.6.

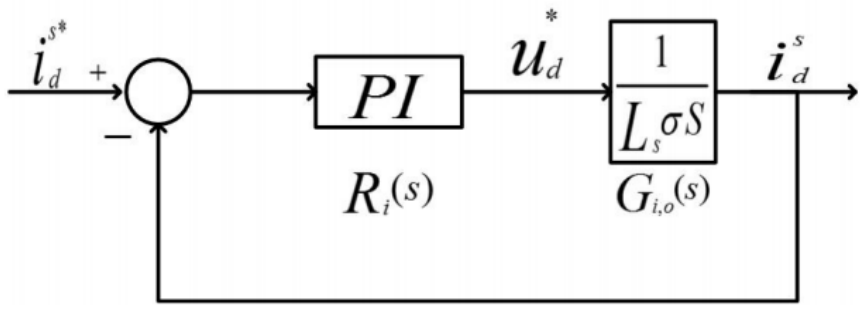

Fig 1.6: The block diagram of the direct axis current control

$$G_{i,o} = R_i(s)G_i(s) = \frac{K_p^i}{L_s\sigma T_i^i}\frac{1}{s^2}(1 + sT_i^i)$$

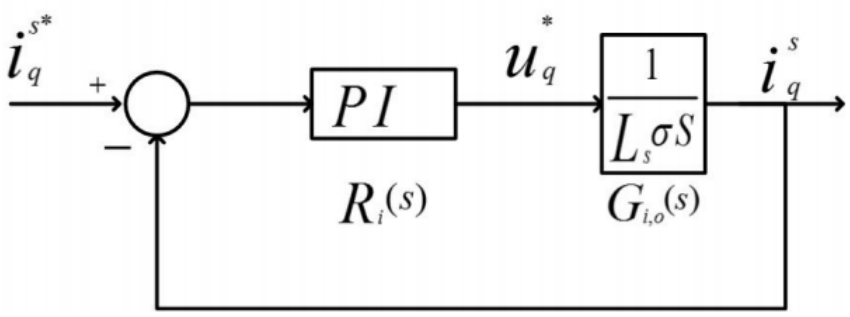

Fig 1.7: The block diagram of the quadrature axis current control

Where K_p^i *and* T_i^i are the corresponding K_p *and* T_i parameters for current PI Controller.

Applying the phase margin condition (1.39) of $G_{i,o}$ we have

$$\arg\left(G_{i,o}(j\omega_c)\right) = tan^{-1}\frac{\omega_c T_i^i}{1} - \pi$$

$$= tan^{-1}(\omega_c T_i^i) - \pi = -\frac{2\pi}{3} \qquad (1.40)$$

Therefore, the T_i^i value can be obtained from

Applying the magnitude condition (1.39) of $G_{i,o}$ and substituting T_i^i value, we get K_p^i.

$$G_{i,o}(j\omega) = \frac{K_p^i}{L_s\sigma T_i^i}\frac{1}{\omega_c^2}\sqrt{1 + (\omega_c T_i^i)^2} = 1$$

$$K_p^i = \frac{L_s\sigma T_i^i\omega_c^2}{\sqrt{1+(\omega_c T_i^i)^2}} \qquad (1.41)$$

Therefore, based on the calculated T_i^i and K_p^i values, we obtain K_i^i from

$$K_i^i = \frac{K_p^i}{T_i^i} \qquad (1.42)$$

The closed loop transfer function can be obtained based on the open loop transfer function $G_{i,o}$, as follows

$$G_{i,c} = \frac{G_{i,o}}{1+G_{i,o}} = \frac{1+sT_i^i}{1+sT_i^i+s^2\frac{T_i^i \sigma L_s}{K_p^i}} \quad (1.43)$$

3.2.2 PI SPEED CONTROLLER DESIGN

In this section, we design the K_p^ω and K_i^ω values for the speed controller using symmetrical optimum method which guarantees the maximum phase margin. First, notice the equation (1.43) is a second-order system, we need to approximate it by simplified first-order transfer function. That significantly simplifies the speed controller design as follows [3].

$$G_{i,c}(s) = G_{i,sim}(s) = \frac{1}{1+\frac{s}{\omega_g}} \quad (1.44)$$

Where $\omega_g = \frac{1}{T_g}$

Since the magnitude of closed loop transfer function decreases by 20 dB/decade for high frequencies, the cut-off frequency of low pass filter can be determined easily. First the frequency ω_1, is chosen as ten times the switching frequency:

$$\omega_1 = 10.f_s.2\pi \quad (1.45)$$

Then, the cutoff frequency ω_g of the simplified transfer function can be obtained by interpolating the Bode plot:

$$-20.\log\left(\frac{\omega_1}{\omega_g}\right) = |G_{i,c}(j\omega_1)| \quad (1.46)$$

Therefore, ω_g can be calculated from

$$\omega_g = 10^{[\log(\omega_1) - \frac{|G_{i,c}(j\omega_1)|}{20}]} \quad (1.47)$$

Therefore, the simplified transfer function (1.44) can be determined with the cutoff frequencyω_g. Based on (3.28), and the load equation

$$T_e - T_L = J\,\dot{\omega}_m \quad (1.48)$$

The open loop transfer function for speed control is given as follows

$$G_{\omega}(s) = G_{i,sim}(s)\frac{3}{2}\frac{P}{2}\frac{L_m}{L_r}\lambda_d^r\frac{1}{sJ} \tag{1.49}$$

Where P is the number of poles.

Now introducing the PI speed controller into the system, the open loop transfer function of the overall plant is shown below :

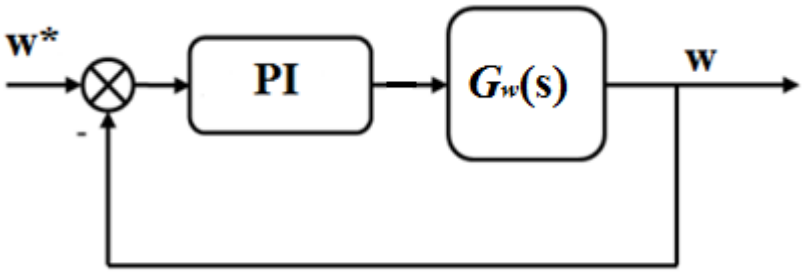

Fig 1.8: The block diagram of the speed control

$$G_{\omega,o}(s) = R_{\omega}(s)G_{\omega}(s)$$

$$= K_p^{\omega}\left(1+\frac{1}{sT_i^{\omega}}\right)\frac{1}{1+\frac{s}{\omega_g}}\frac{3}{2}\frac{P}{2}\frac{L_m}{L_r}\lambda_d^r\frac{1}{s.J}$$

$$= K_p^{\omega}\left(1+\frac{1}{sT_i^{\omega}}\right)\left(\frac{1}{s+\frac{s^2}{\omega_g}}\right)\frac{3PL_m\lambda_d^r}{4L_rJ}$$

$$= K_p^{\omega}\frac{3PL_m\lambda_d^r}{4L_rJ}\frac{1+sT_i^{\omega}}{sT_i^{\omega}\left(s+\frac{s^2}{\omega_g}\right)} \tag{1.50}$$

The symmetrical optimum method is used for determining the parameters of the PI speed controller. The method can produce the balance phase and magnitude characteristic of the open loop transfer function, by placing the crossover frequency precisely at the location where we can obtain the maximum phase margin. The slope of -20 dB/decade produced by PI controller becomes -40 dB/decade after the cutoff frequency ω_g of current control loop low-filter.

We introduce the factor α that relates the cross-over frequency ω_c and PI speed controller cutoff frequency ω_w with the first-order system cutoff frequency ω_g, where

$$\omega_c = \frac{1}{\alpha}\omega_g, \omega_w = \frac{1}{\alpha^2}\omega_g$$

On logarithmic scale ω_c is exactly the middle point between ω_w and ω_g. Applying these two conditions to the open loop transfer function, we have:

$$|(G_{w,o}(j\omega_c)| = \left|G_{w,o}\left(\frac{j\omega_g}{\alpha}\right)\right| = 1 \tag{1.51}$$

$$\arg\left(G_{w,o}(j\omega_c)\right) = \arg\left(G_{w,o}\left(\frac{j\omega_g}{\alpha}\right)\right) = -\frac{2\pi}{3} \tag{1.52}$$

Firstly, α is solved from the phase margin condition, i.e.

$$\arg\left(G_{w,o}(j\omega_c)\right) = \arg(1 + j\omega_c T_i^w) - \arg\left(1 + j\omega_c T_g\right) - \pi$$

$$= tan^{-1}(\omega_c T_i^w) - tan^{-1}\left(\omega_c T_g\right) - \pi \tag{1.53}$$

Since $\omega_c = \frac{1}{\alpha}\omega_g = \frac{1}{\alpha T_g}$ and $T_i^w = \alpha^2 T_g$ we get,

$$tan^{-1}(\alpha) - tan^{-1}\left(\frac{1}{\alpha}\right) = \frac{\pi}{3} \tag{1.54}$$

Based on trigonometric rules, we can obtain the value of α. The controller parameter K_p^w can be determined by substituting α in the magnitude condition (1.51).

$$\left|G_{w,o}\left(\frac{j\omega_g}{\alpha}\right)\right| = \left|G_{w,o}\left(\frac{1}{j\alpha T_g}\right)\right| = K_p^\omega \frac{3PL_m\lambda_d^r}{4L_rJ} T_g \sqrt{\frac{1+\alpha^2}{1+\frac{1}{\alpha^2}}} = 1$$

$$K_p^\omega = \frac{1}{\frac{3PL_m\lambda_d^r}{4L_rJ} T_g \sqrt{\frac{1+\alpha^2}{1+\frac{1}{\alpha^2}}}} \tag{1.55}$$

Therefore, based on the calculated T_i^ω and K_p^ω value, we can obtain K_i^ω from

$$K_i^\omega = \frac{K_p^\omega}{T_i^\omega} \tag{1.56}$$

1.3 Simulation

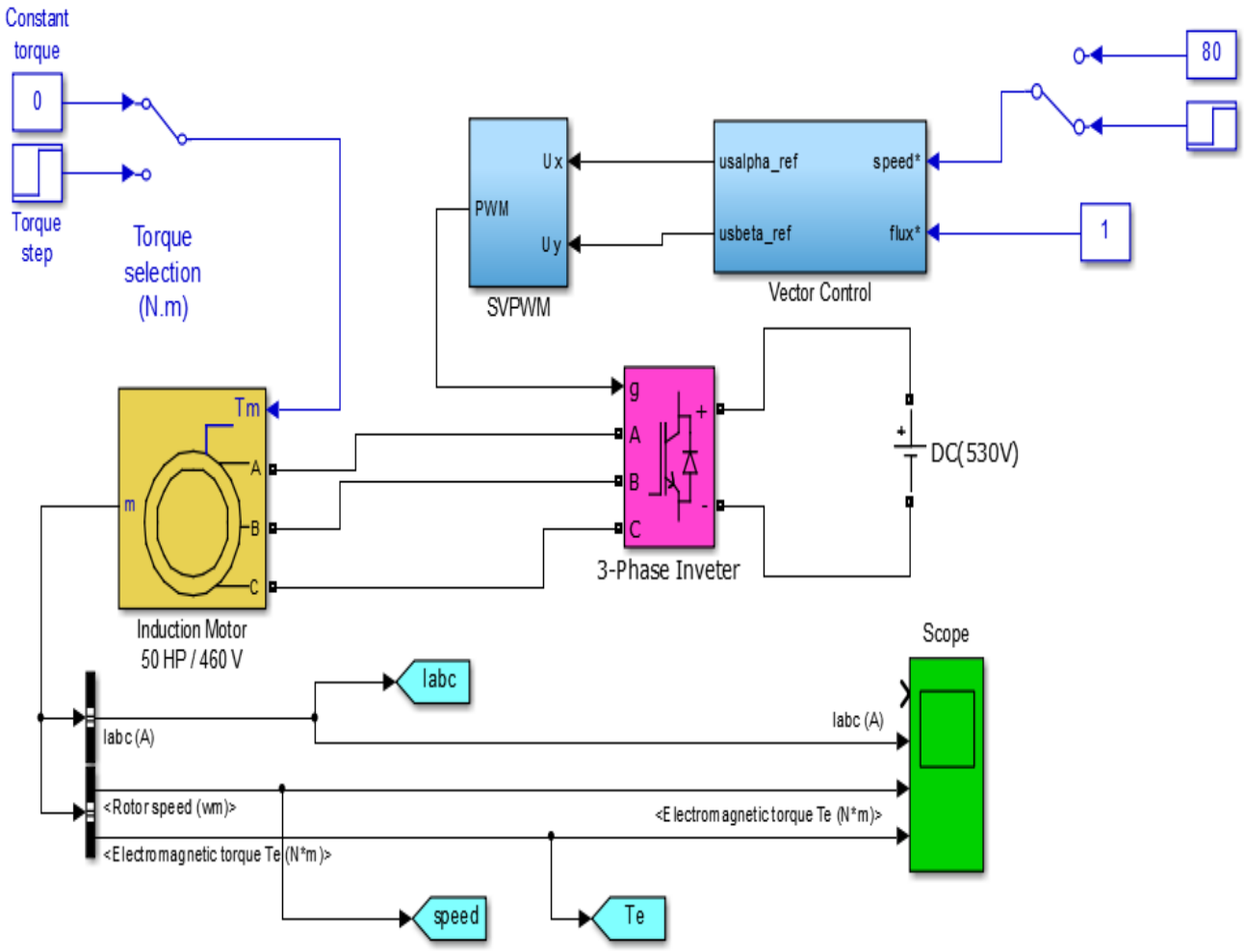

Fig 1.9: FOC Simulink Model

The proposed control system has been simulated using Matlab/Simulink, a sensorless induction motor drive simulation was setup.

The FOC model contains four main sub-blocks (Induction motor, 3-phase Inverter, SVPWM and vector control).

In order to generate the regulated voltage the reference values such as speed and flux are injected in the vector control sub block, also the actual speed and current values are used from the motor outputs.

In the SVPWM sub-block the regulated voltages are used to generate the six pwm to control the inverter.

The inverter drives the motor with the controlled abc voltage to reach the desired speed.

Scenario 1

The speed reference is set at 80 rad/s, at t=1.5 s the speed reference is set to 160 rad/s and the load torque is set to 0 (no load).

The results are shown in Fig 1.10:

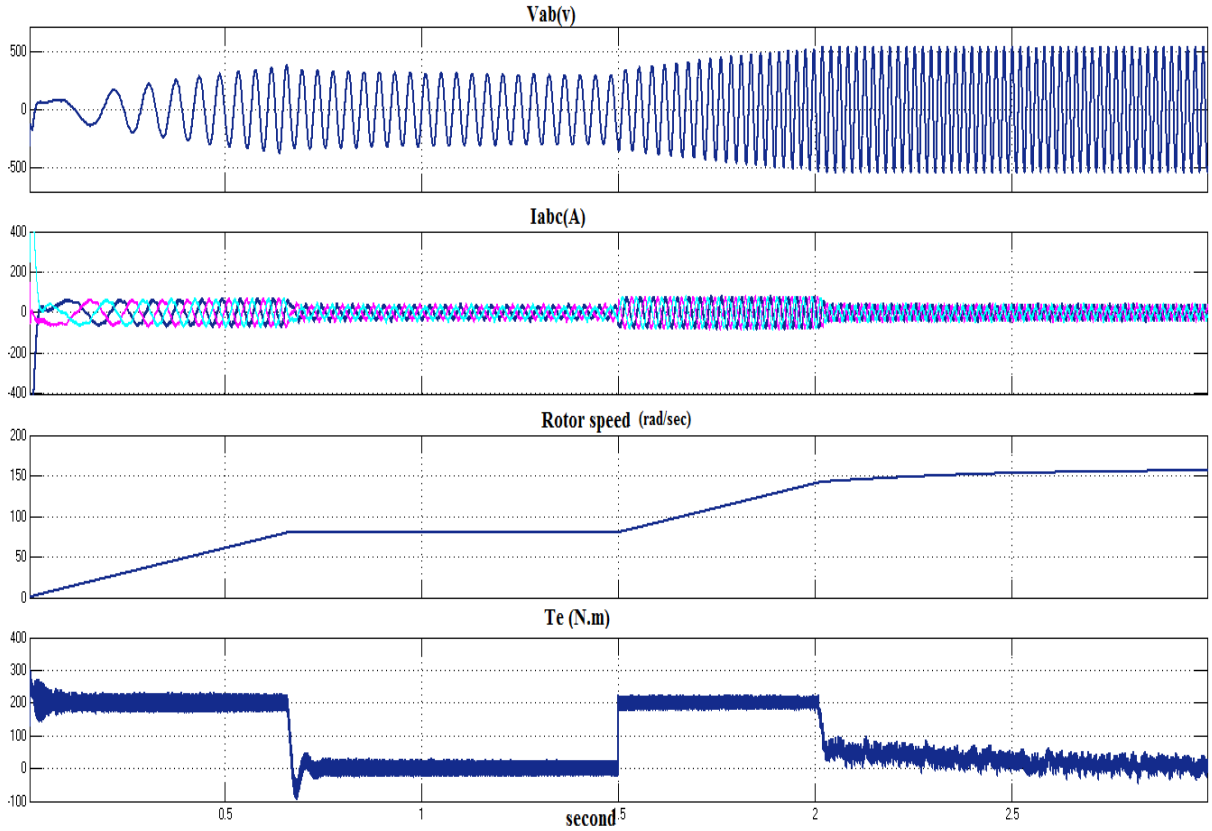

Fig 1.10: Test results for scenario 1.

First, it is important to analyze the starting performance. During this starting period, the electric motor needs to produce a relatively high torque in a very short time to accelerate itself. The investigation here is focused on speed response time and fluctuations.

For the torque responses, at first, a large torque is generated to start the motor. After reaching the target speed, the torque output follows the command closely.

Since the FOC is aimed for controlling the decoupled currents Iqs and Ids of the system, so generally speaking, the currents are well regulated. It can be seen that, at the starting stage, three phase currents are constrained within -50 to +50 Amps. After that, the magnitude of the current is kept around 20 Amps.

A ramp signal is used to simulate the vehicle starting speed behavior, after the motor speed has reached the target value of 80 rad/s, it was kept as a constant. At t=1.5s, the speed is increased from 80 to 160 rad/s.

Scenario 2

The speed reference is set at 80 rad/s. The torque load is set to 0 (no load) at t=1 s the torque load is set to 50 N.m.

The results are shown in Fig 1.11:

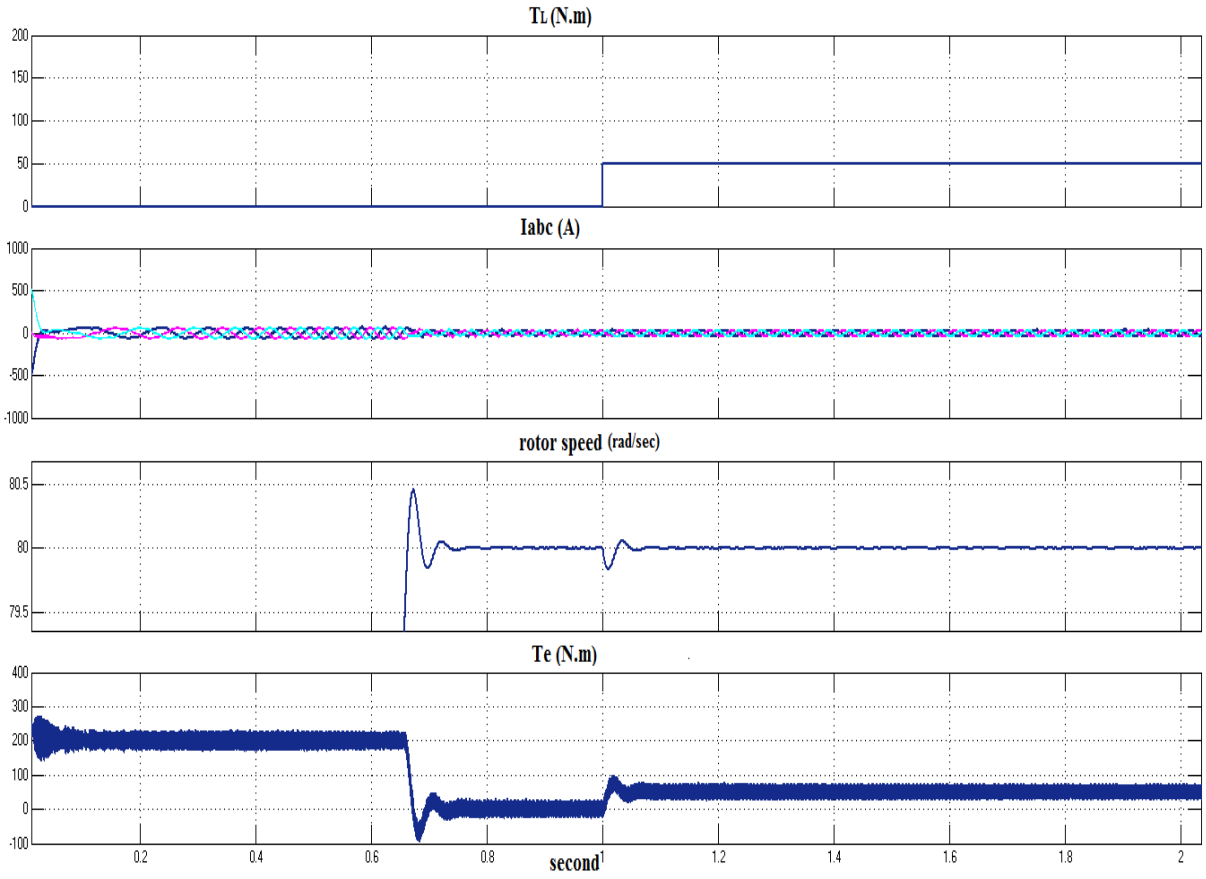

Fig 1.11: Test results for scenario 2

When the vehicle is running at a constant speed, the load on the motor can vary abruptly because of the change of the road conditions. In this scenario, the speed is kept constant all the time and load torque is varied.

For the torque responses, at first, a large torque is generated to start the motor. After reaching the target speed, the torque output follows the command closely during the constant speed

period. The load was changed at t=1s from 0 Nm to 50 Nm, it can be seen that the load torque is suddenly changed, there is a small speed dip, but it is restored quickly.

From the zoomed pictures of speed response, we can see that at the time t = 1s, the speed response of FOC follows the command very closely and the overshoot is almost 0.

From the zoomed picture of torque response, it can be seen clearly that the torque fluctuations of FOC are restrained within +20 and -20 (Nm).

Scenario 3

The speed reference is set at 80 rad/s, at t=1.5 s the speed reference is set to 160 rad/s.

The torque load is set to 0 (no load) at t=1 s the torque load is set to 50 N.m.

In this scenario we mixed the two previous scenarios. The results are shown in Fig 1.12:

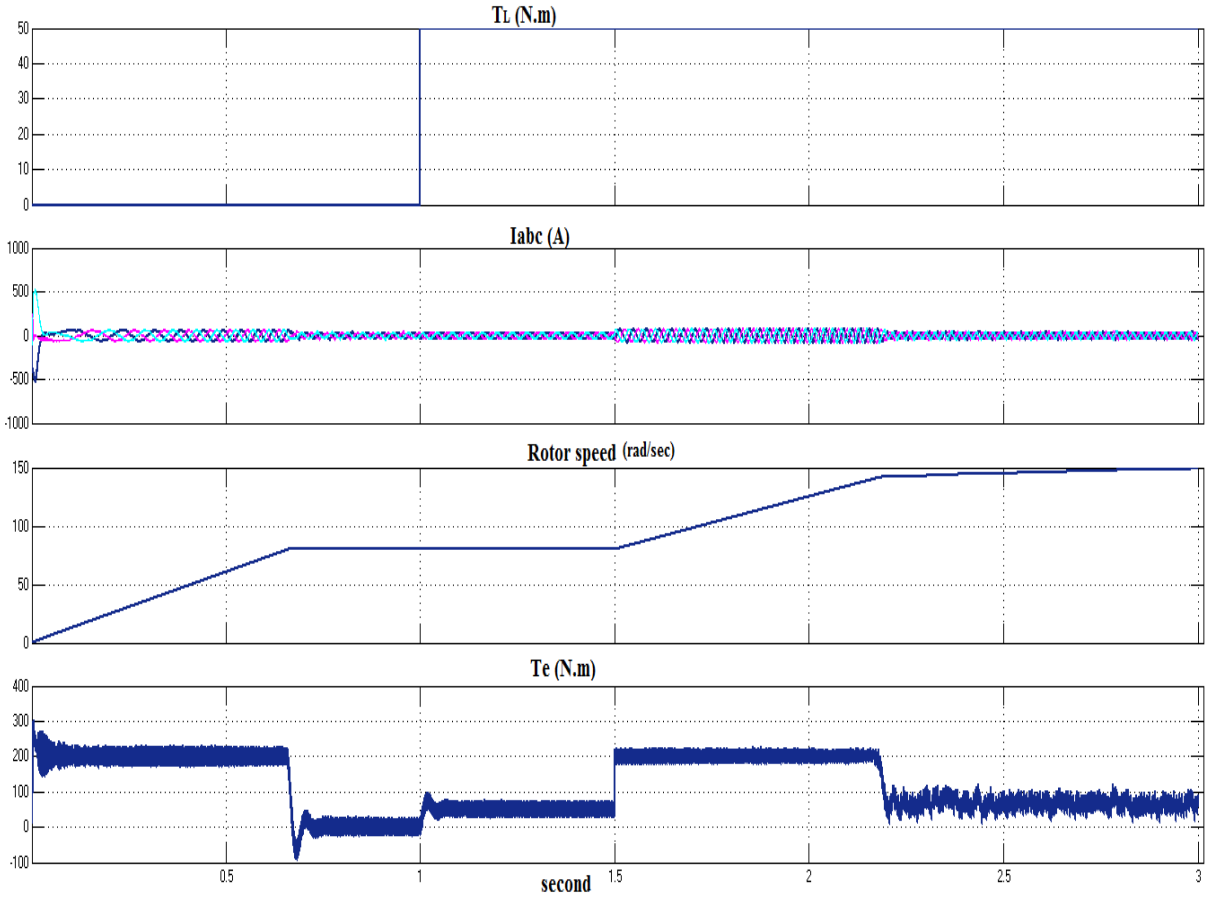

Fig 1.12: Test results for scenario 3.

1.4 Conclusion

In this chapter the concept and the model of field oriented control were presented. The feed-forward control method is designed for decoupling the torque and flux. The effectiveness of the proposed control scheme of induction motor control was demonstrated by computer simulations. The simulation results show the robustness and effectiveness of the designed controllers.

CHAPTER 2

SPEED ESTIMATOR

2.1 Introduction

The use of sensorless control of the induction machine, vector controlled IM drives without a speed sensor has become an attractive technology.

The absence of the mechanical speed sensor improves the ruggedness of the drive and reduces the cost and the volume of the assembly. The problem was largely studied by researchers and has commercial applications especially for motors running at medium or high speeds. At low-speed, however, it is still problematic to achieve robust control. The idea of sensorless control is presented in this chapter.

2.2 Data acquisition

Taking measurements using conventional meters is very slow and is able to show only the steady state values. For a fast data acquisition system fast sensors are required to track the change in the measured quantities. The voltage, current and speed of the induction machine are measured using appropriate sensors to be processed in the Digital Signal Processing part for machine analysis and control[4].

2.3 Speed measurement

Speed measurements were obtained from the built in optical encoder. The optical encoder's disc is made of plastic with transparent and opaque areas. A light source and photo detector array reads the optical pattern which result from the disc's position at any one time. Two output signals are generated from the optical encoder and usually two output waveforms are 90 degrees out of phase, which indicates the rotational direction. The signals can be read by QEP module on DSP, so that the angular speed of the motor shaft can be calculated in software easily.

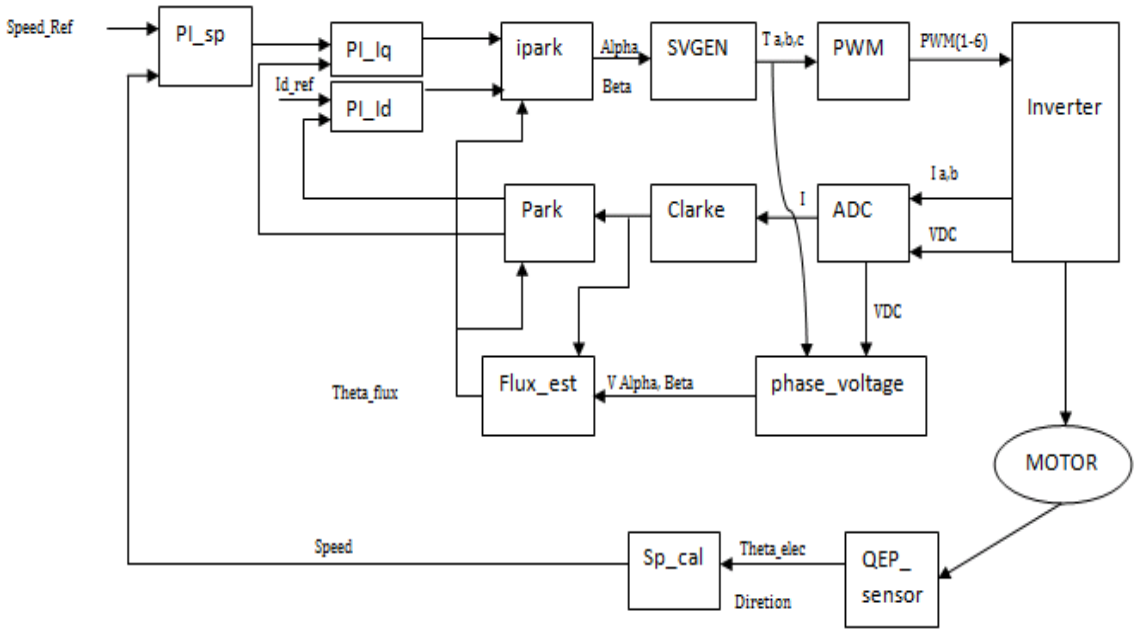

Fig 2.1: Design of vector control PWM for induction motor

The enhanced quadrature encoder pulse (eQEP) module of the F28335 is used to process the digital signal form the encoder built on top of the motor [5]. There are four different modes in which the quadrature module is able to run. They are quadrature mode, direct count mode, up count and down count mode. In quadrature mode, the eQEP module receives two square wave signals from the encoder. These two square wave signals (A and B) have 90° phase shift with respect to each other. In direction-count mode, one square wave signal and one direction signal are sent to the eQEP module. The counter in the module will increase or decrease depending on the direction. For both modes, an index pulse signal is used to determine the absolute position of the encoder. The operating mode of the eQEP module is selected by the type of encoder. As the incremental encoder is used in this project outputs the quadrature signals, the eQEP module is set to be working in quadrature-count mode. The general block diagram of eQEP module is shown in Fig2.2 which shows the functionality of the encoder.

Two quadrature waves are sent to the QA pin and QB pin of the decoder block as shown in the Fig 2.3. Every falling or rising edge of QA and QB will generate a clock signal (QCLK), which is passed to the position counter (QPOSCNT) from the decoder. The QPOSCNT will increase or decrease by 1 unit on each pulse of QCLK, depending on the direction signal (QDIR).

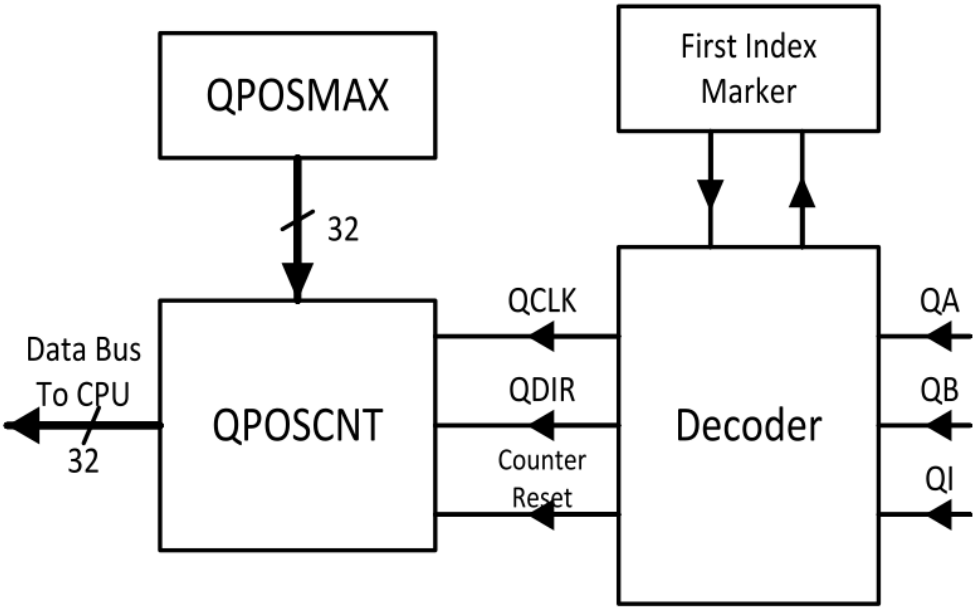

Fig 2.2: Block diagram of eQEP module [4]

The following Table 1 shows the details of the values of QDIR and QPOSCNT. Fig 3 shows the example waveform of the eQEP, which has the quadrature QA, QB pins and index pulses. Every time the position counter (QPOSCNT) is reset by the index signal. When it meets the index signal for the first time, the eQEP module will remember the present edge and the rotating direction in the first index marker register.

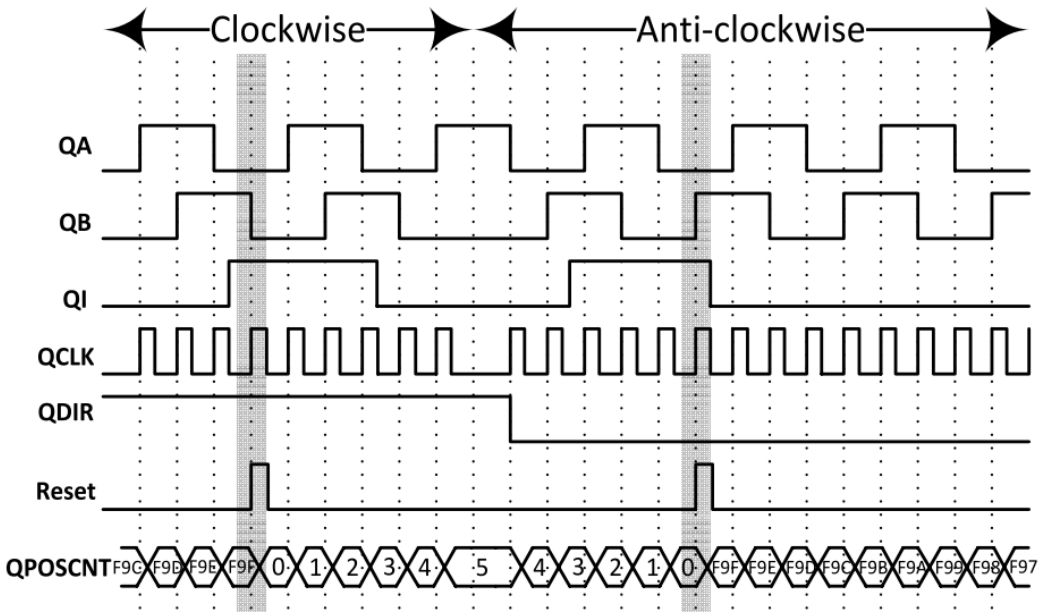

Fig 2.3: Example waveforms of the eQEP.

Tab2.1: Encoder Truth table

Previous edge	Present edge	QDIR	QPOSCNT
QA↑	QB↑	1	increment
	QB↓	0	decrement
	QA↓	TOGGLE	increment or decrement
QA↓	QB↓	1	increment
	QB↑	0	decrement
	QA↑	TOGGLE	increment or decrement
QB↑	QA↑	0	decrement
	QA↓	1	increment
	QB↓	TOGGLE	increment or decrement
QB↓	QA↓	0	decrement
	QA↑	1	increment
	QB↑	TOGGLE	increment or decrement

The speed information is determined by counting the number of pulses, which represent an increment in angular position, during a specified sampling period. The 5000 line encoder gives 20000 measuring steps per revolution. In general the speed resolution is expressed as

$$\omega_{res} = \frac{\theta_{res}}{T_s} \qquad (2.1)$$

Where θ_{res} is incremental angular position resolution equal to $5x10^{-5}$ of a revolution $=3.142x10^{-4}$ radians.

T_s is the sampling period (seconds).

Hence the speed resolution expressed in revolutions per minute (rpm) is

$$\omega_{res} = \frac{5\times10^{-5}}{T_s} \times 60 = \frac{0.003}{T_s}\ rpm \qquad (2.2)$$

With a sampling time of 200μsec (Ts = 200μs) the speed resolution will be 15rpm. This means that the speed measurement is expressed as a discrete value in 15rpm steps. The maximum error, irrespective of the speed, will be 15*rpm*. At high speed the relative error in speed measurement is small however at low speed the relative error is large. If the sampling time is 500μs then the speed resolution is 6rpm. For a sampling time of

1ms the speed resolution is 3*rpm*.

The accuracy of speed measurement depend on the sampling time. The sampling time has to be large enough so that the accuracy of the speed measurement will be improved. However the sampling time should not be increased to an extent where it will not be able to follow the change in speed quickly and affect a control system dependent on rotor speed.

2.4 Speed estimator

Technical Background

The open-loop speed estimator is derived basically from the mathematics equations of induction motor in the stationary reference frame. The precise values of machine parameters are unavoidably required, otherwise a steady-state speed error may happen. However, the structure of the estimator is much simple comparing with other advanced techniques. All equations represented here are in the stationary reference frame ($\omega_s = 0$) (with superscript "s"). Firstly, the rotor flux linkage equations can be shown as below:

$$\lambda^s_d = L_s\, i^s_d + L_m\, i^r_d \qquad (2.3)$$

$$\lambda^s_q = L_s\, i^s_q + L_m\, i^r_q \qquad (2.4)$$

where Lr, and Lm are rotor, and magnetizing inductances respectively. According to equations (2.3) and (2.4), the rotor currents can be expressed as :

$$i^s_{dr} = \frac{1}{L_r}(\lambda^s_{dr} - L_m\, i^s_{ds}) \qquad (2.5)$$

$$i^s_{qr} = \frac{1}{L_r}(\lambda^s_{qr} - L_m\, i^s_{qs}) \qquad (2.6)$$

Secondly, the rotor voltage equations are used to find the rotor flux linkage dynamics.

$$0 = r_r\, i^r_d + \omega_r \lambda^r_q + \frac{d}{dt}\lambda^r_d \qquad (2.7)$$

$$0 = r_r\, i^r_q - \omega_r \lambda^r_d + \frac{d}{dt}\lambda^r_q \qquad (2.8)$$

Where ω_r is electrical angular velocity of rotor (rad/sec), and Rr is rotor resistance (Ω). Substituting the rotor currents from (2.5) and (2.6) into (2.7) and (2.8), then the rotor flux linkage dynamics can be found as:

$$\frac{d\lambda_{dr}^{s}}{dt} = -\frac{1}{\tau_r}\lambda_{dr}^{s} + \frac{L_m}{\tau_r}\mathrm{i}_{ds}^{s} - \omega_r\lambda_{qr}^{s} \quad (2.9)$$

$$\frac{d\lambda_{qr}^{s}}{dt} = -\frac{1}{\tau_r}\lambda_{qr}^{s} + \frac{L_m}{\tau_r}\mathrm{i}_{qs}^{s} - \omega_r\lambda_{qr}^{s} \quad (2.10)$$

Where τ_r = Lr/Rr is rotor time constant (sec).

Suppose that the rotor flux linkages in (2.9) and (2.10) are known, therefore, their magnitude and angle can be computed as follows

$$\lambda_r^s = \sqrt{(\lambda_{dr}^s)^2 + (\lambda_{qr}^s)^2} \quad (2.11)$$

$$\theta_{\lambda_r} = tan^{-1}\left(\frac{\lambda_{qr}^s}{\lambda_{dr}^s}\right) \quad (2.12)$$

Next, the rotor flux (i.e., synchronous) speed, ω_e can be easily calculated by derivative of the rotor flux angle in (2.12).

$$\omega_e = \frac{d\theta_{\lambda_r}}{dt} = \frac{d(tan^{-1}\left(\frac{\lambda_{qr}^s}{\lambda_{dr}^s}\right))}{dt} \quad (2.13)$$

Referring to the derivative table, equation (2.13) can be solved as

$$\frac{d(tan^{-1}u)}{dt} = \frac{1}{1+u^2}\frac{du}{dt} \quad (2.14)$$

Where $u = \left(\frac{\lambda_{qr}^s}{\lambda_{dr}^s}\right), yields$

$$\omega_e = \frac{d\theta_{\lambda_r}}{dt} = \left(\frac{(\lambda_{dr}^s)^2}{(\lambda_r^s)^2}\right)\left\{\frac{\lambda_{dr}^s\frac{d\lambda_{qr}^s}{dt} - \lambda_{qr}^s\frac{d\lambda_{dr}^s}{dt}}{(\lambda_{dr}^s)^2}\right\} \quad (2.15)$$

Substituting (2.9) and (2.10) into (2.15), and rearranging, then finally it gives:

$$\omega_e = \frac{d\theta_{\lambda_r}}{dt} = \omega_r + \frac{1}{(\lambda_r^s)^2}\frac{L_m}{\tau_r}(\lambda_{dr}^s\,\mathrm{i}_{qs}^s - \lambda_{qr}^s\,\mathrm{i}_{ds}^s) \quad (2.16)$$

The second term of the left hand in (2.16) is known as slip that is proportional to the electromagnetic torque when the rotor flux magnitude is maintained constant. The electromagnetic torque can be shown here for convenience.

$$\mathrm{T_e} = \frac{\mathrm{P}}{2}\frac{3}{2}\frac{\mathrm{L_m}}{\mathrm{L_r}}(\lambda_{\mathrm{d}}^{\mathrm{r}}\mathrm{i}_{\mathrm{q}}^{\mathrm{s}} - \lambda_{\mathrm{q}}^{\mathrm{r}}\mathrm{i}_{\mathrm{d}}^{\mathrm{s}}) \quad (2.17)$$

Where p is the number of poles. Thus, the rotor speed can be found as

$$\omega_r = \omega_e - \frac{1}{(\lambda_r^s)^2}\frac{L_m}{\tau_r}(\lambda_{dr}^s \mathrm{i}_{qs}^s - \lambda_{qr}^s \mathrm{i}_{ds}^s) \qquad (2.18)$$

Now, the per-unit concept is applied to (2.18), then, the equation (2.18) becomes

$$\omega_{r,pu} = \omega_{e,pu} - \frac{1}{(\lambda_{r,pu}^s)^2}\frac{1}{\omega_b \tau_r}\left(\lambda_{dr,pu}^s \mathrm{i}_{qs,pu}^s - \lambda_{qr,pu}^s \mathrm{i}_{ds,pu}^s\right) \quad pu \qquad (2.19)$$

where $\omega_b = 2\pi f$ is the base electrically angular velocity (rad/sec), $\lambda_b = L_m I_b$ is the base flux linkage (volt.sec), and I_b is the base current (amp). Equivalently, another form is

$$\omega_{r,pu} = \omega_{e,pu} - \frac{1}{(\lambda_{r,pu}^s)^2} K_1\left(\lambda_{dr,pu}^s \mathrm{i}_{qs,pu}^s - \lambda_{qr,pu}^s \mathrm{i}_{ds,pu}^s\right) \quad pu \qquad (2.20)$$

Where $K_1 = \frac{1}{\omega_b \tau_r}$.

The per-unit synchronous speed can be calculated as

$$\omega_{e,pu} = \frac{1}{2\pi f_b}\frac{d\theta_{\lambda_r}}{dt} = \frac{1}{f_b}\frac{d\theta_{\lambda_r,pu}}{dt} \quad pu \qquad (2.21)$$

where f_b is the base electrical (supplied) frequency (Hz) and 2π is the base angle (rad).

Discretizing equation (2.21) by using the backward approximation, yields

$$\omega_{e,pu}(k) = \frac{1}{f_b}\left(\frac{\theta_{\lambda_r,pu}(k) - \theta_{\lambda_r,pu}(k-1)}{T}\right) \quad pu \qquad (2.22)$$

Where T is the sampling period (sec). Equivalently, another form is

$$\omega_{e,pu}(k) = K_2(\theta_{\lambda_r,pu}(k) - \theta_{\lambda_r,pu}(k-1)) \quad pu \qquad (2.23)$$

Where $K_2 = \frac{1}{f_b T}$ is usually a large number.

In practice, the typical waveforms of the rotor flux angle, $\theta_{\lambda,pu}$, in both directions can be seen in Fig 2.4. To take care of the discontinuity of angle from 360° to 0°(CCW) or from 0° to 360° (CW), the differentiator is simply operated only within the differentiable range as seen in this Figure 2.4. This differentiable range does not significantly lose the information to compute the estimated speed.

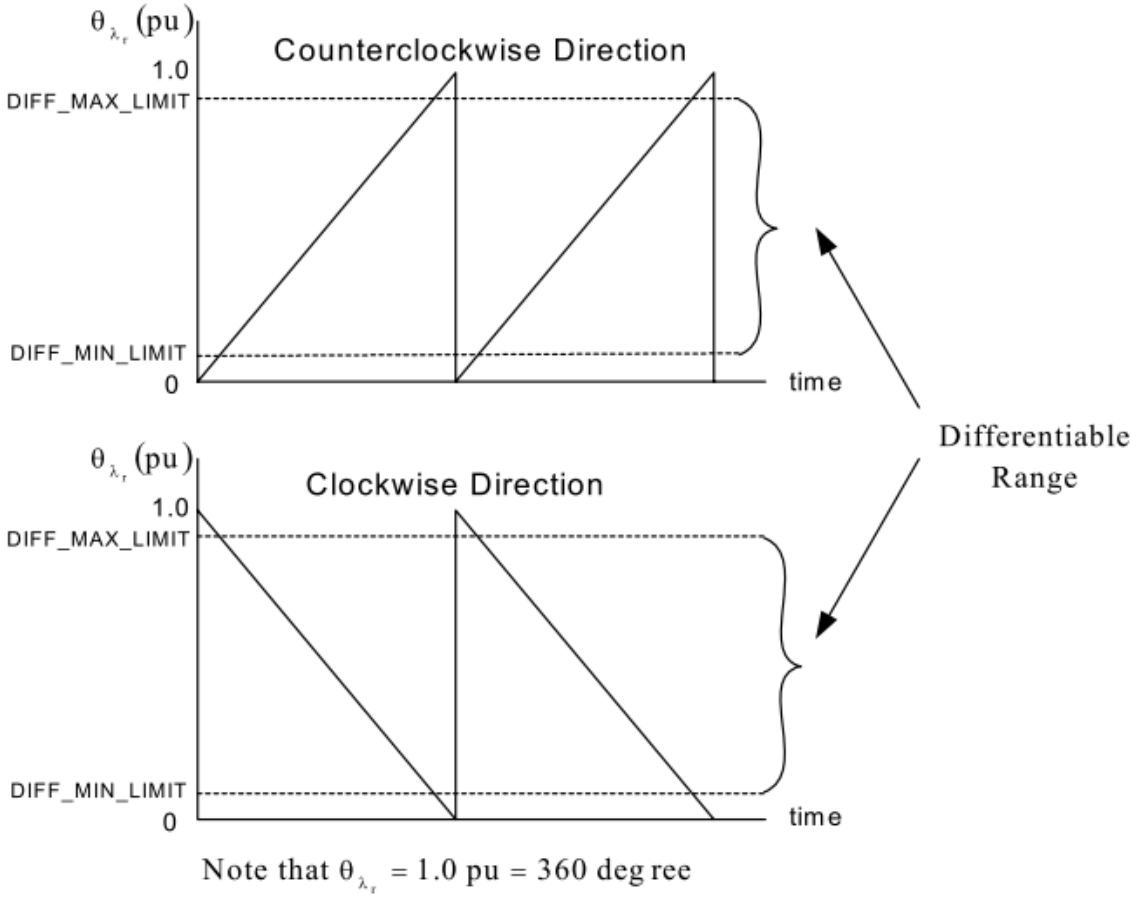

Fig 2.4: The waveforms of rotor flux angle in both directions

In addition, the synchronous speed in (2.23) is necessary to be filtered out by the low-pass filter in order to reduce the amplifying noise generated by the pure differentiator in (2.23). The simple 1st-order low-pass filter is used, then the actual synchronous speed to be used is the output of the low-pass filter, $\widehat{\omega}_{e,pu}$, seen in the following equation. The continuous-time equation of 1st-order low-pass filter is as

$$\frac{d\widehat{\omega}_{e,pu}}{dt} = \frac{1}{\tau_c}\left(\omega_{e,pu} - \widehat{\omega}_{e,pu}\right) \qquad pu \qquad (2.24)$$

Where $\tau_c = 1/2\pi f_c$ is the low-pass filter time constant (sec), and f_c is the cut-off frequency (Hz). Using backward approximation, then (2.24) finally becomes

$$\widehat{\omega}_{e,pu}(k) = K_3\widehat{\omega}_{e,pu}(k-1) - K_4\omega_{e,pu}(k) \qquad pu \qquad (2.25)$$

Where $K_3 = \frac{\tau_c}{\tau_c+T}$, and $K_4 = \frac{T}{\tau_c+T}$

In fact, only three equations (2.20), (2.23), and (2.25) are mainly employed to compute the estimated speed in per-unit. The required parameters for this module are summarized as follows:

- The machine parameters:

- number of poles (p)

- rotor resistance (R_r)

- rotor leakage inductance (L_{rl})

- magnetizing inductance (L_m)

- The based quantities:

- base current (I_b)

- base electrical angular velocity (ω_b)

- The sampling period:

- sampling period (T)

- Low-pass filter:

- cut-off frequency (f_c)

Notice that the rotor self inductance is $L_r = L_{rl} + L_m$

Next, Table 2.2 shows the correspondence of notations between variables used here and variables used in the program (i.e., aci_se.c, aci_se.h). The software module requires that both input and output variables are in per unit values.

Tab 2.2:correspondence of notations

	Equation variables	Program variables
Input	λ_{dr}^{s}	PsiDrS
	λ_{qr}^{s}	PsiQrS
	θ_{λ_r}	ThetaFlux
	i_{ds}^{s}	IDsS

	λ_{qs}^{s}	IQsS
Output	ω_r	WrHat
Others	$(\lambda_{dr}^{s})^2$	SquaredPsi
	ω_e	WPsi

This software module implements a speed estimator of the 3-ph induction motor based upon its mathematics model. The estimator accuracy relies heavily on the knowledge of the critical motor parameters

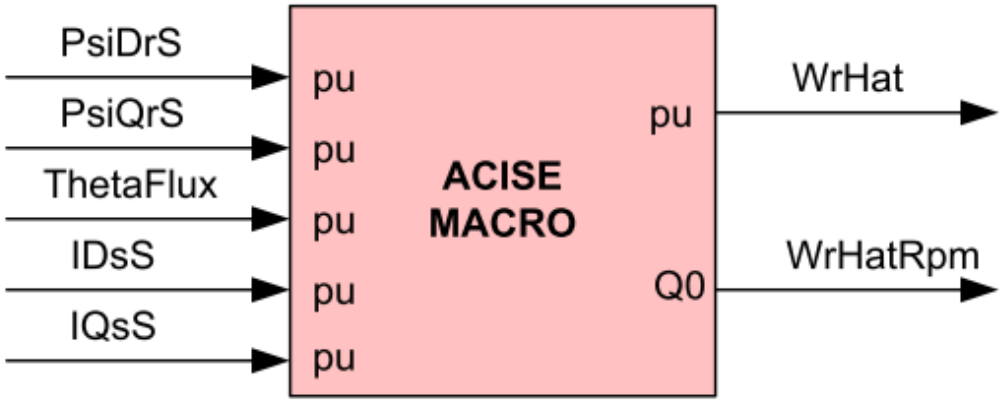

Fig 2.5:Speed_estimator block

.

Analysis of Results

One of the advantages of the setup we use in this project is that the user is able to access the memory, while the processor is still running

The ADC provides the current values Ia and Ib then by using clarke and park transformations these currents are transformed to Id and Iq.

The Id and Iq are injected in the PI regulator and transformed to Clarke voltage by using inverse park transformation (V_α and V_β). The Clarke voltages (V_α and V_β) are shown in Fig2.6.

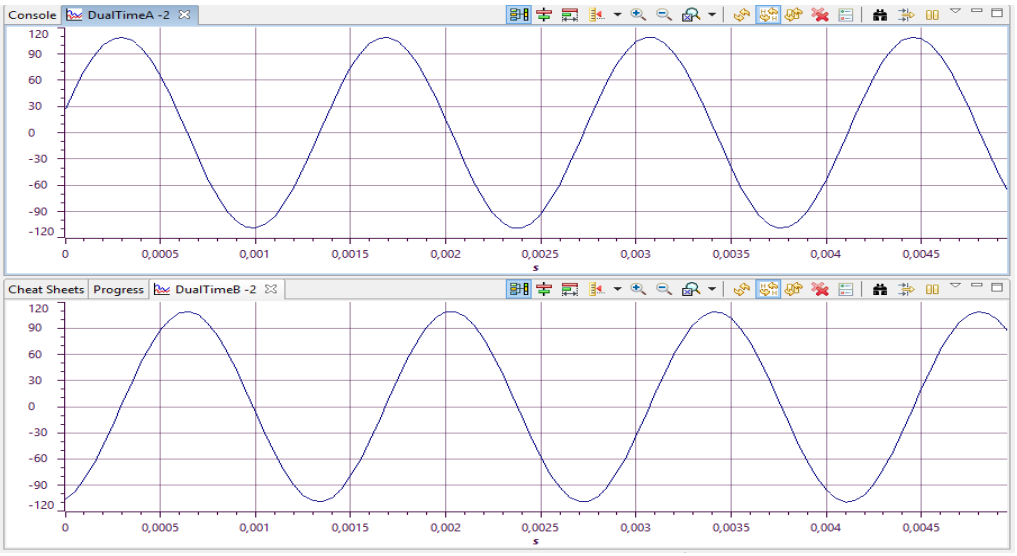

Fig 2.6: Clarke voltage (V_α and V_β).

V_α and V_β are injected in SVGEN module to get the duty cycles as shown in Fig 2.7

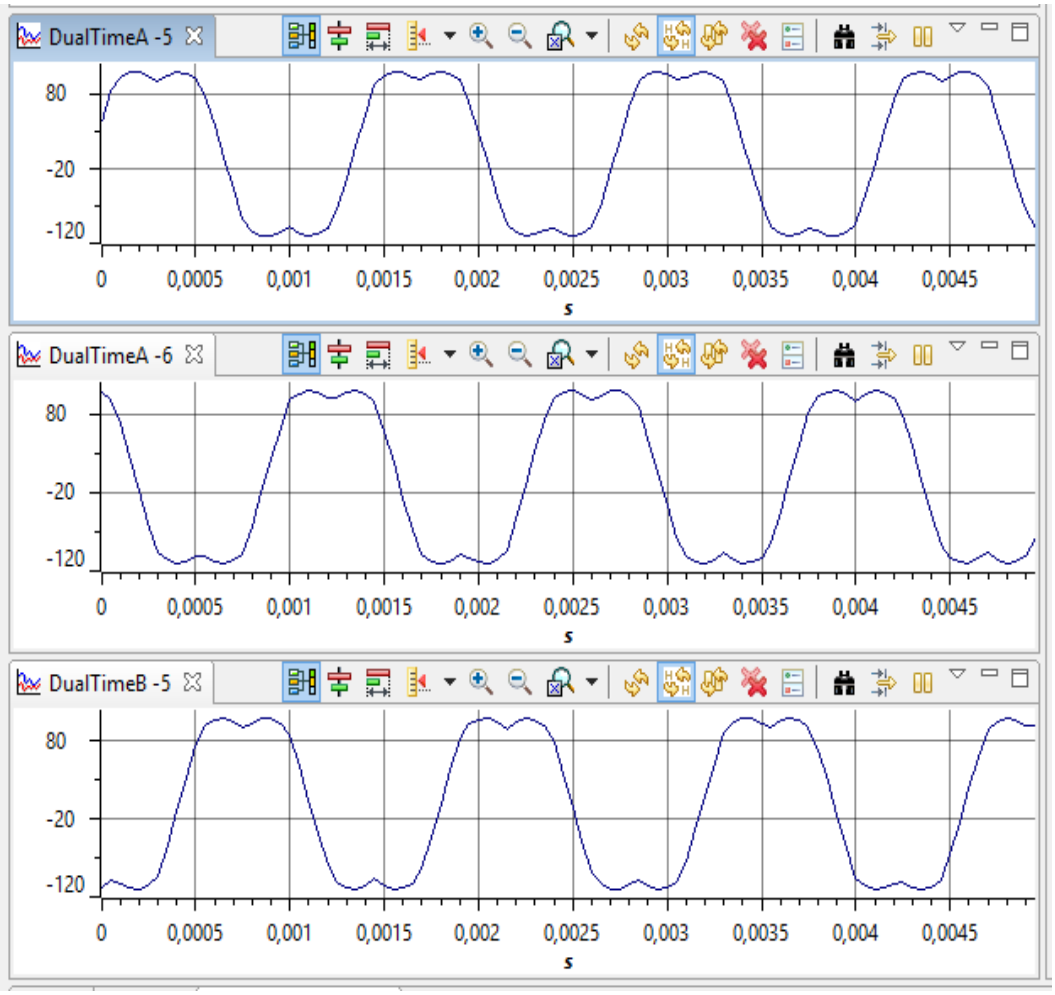

Fig 2.7: Duty cycles (Ta,Tb,Tc)

The duty cycles are used by the PWM sub-block to generate the six pwms (pwm1~pwm6) that control the six gates of the inverter. After that the inverter feeds the motor by the controlled voltages Vabc to reach the target speed.

Fig 2.8 shows the three upper pwms.

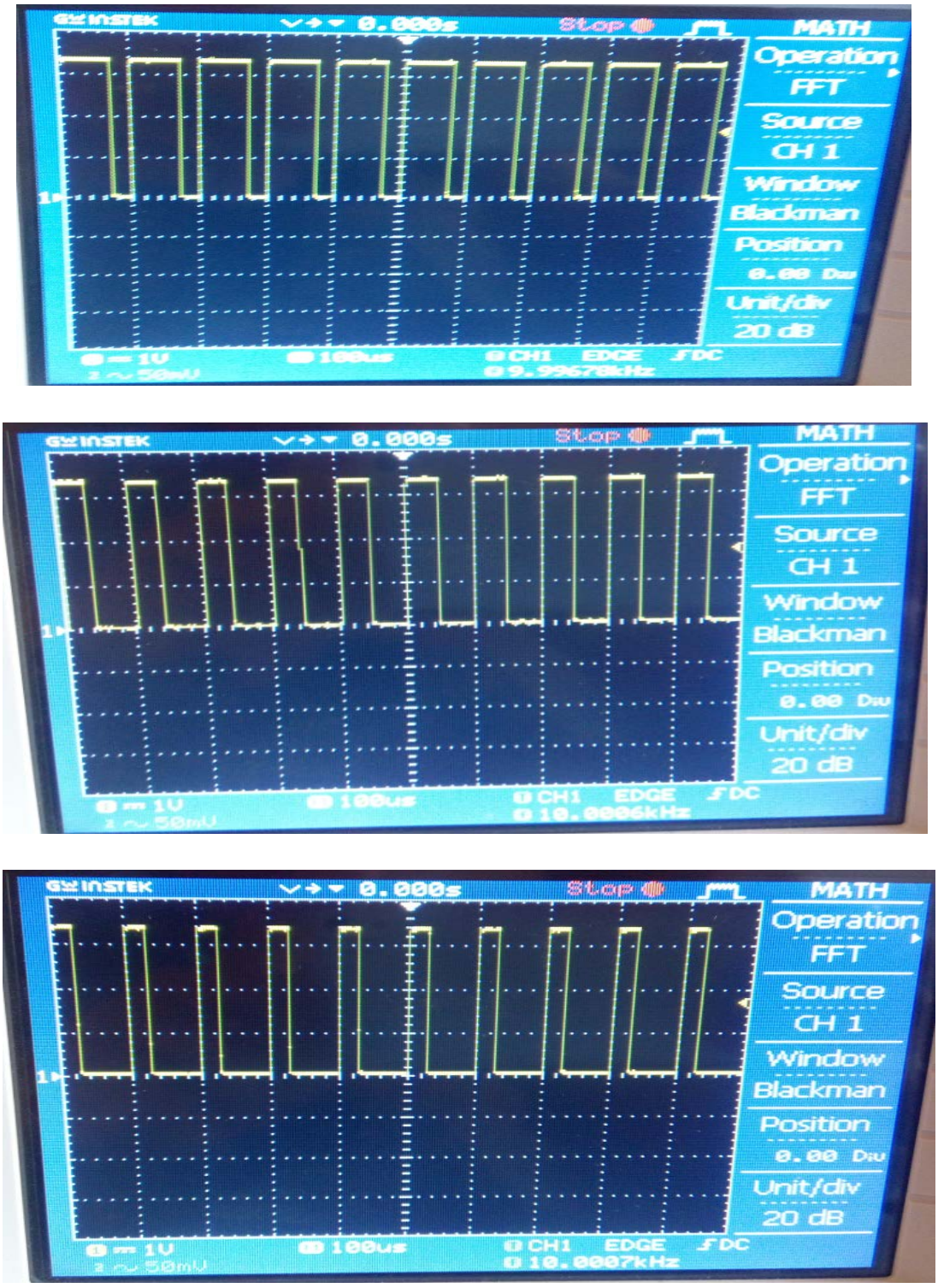

Fig 2.8: the three uppers PWM signals

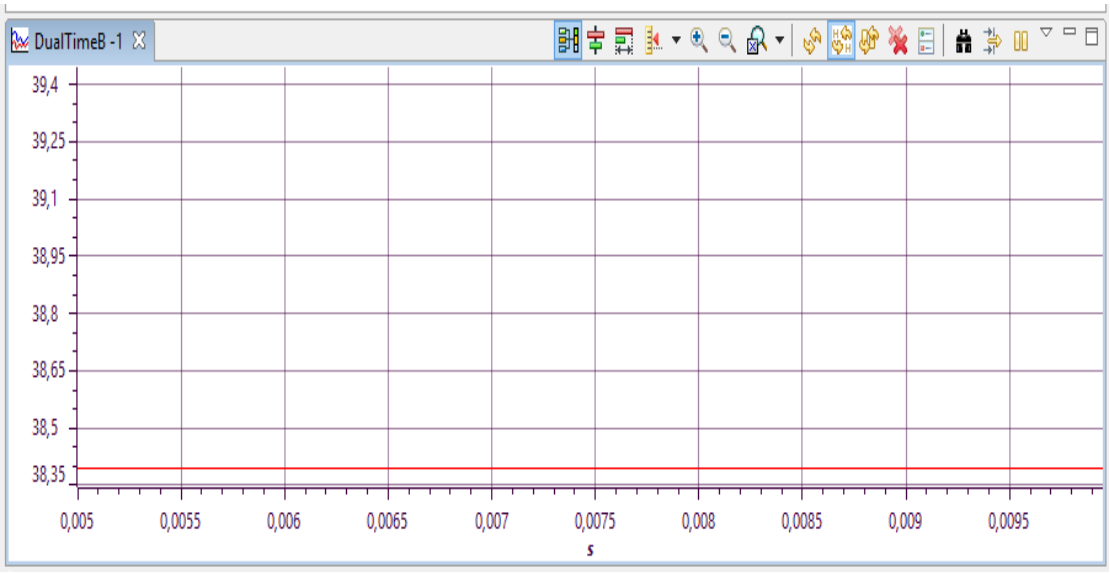

Fig 2.9: The Motor speed

The speed is kept constant at 38.4 rad/s.

In our experimental test the currents loaded have the same values that explains the results obtained in Fig 2.9.

This test was carried out just to prove that our FOC program works and gives the right results.

2.5 Summary

The tested FOC program has shown good performances. If we used the real current signals from ADC, we will have some noise added to the measured signals. For the vector control design, the control system on the DSP manages to control the d,q currents and speed accurately. We notice also from the simulation that the FOC algorithm presents good results, the motor always reach the desired value whatever the load torque value.

conclusion

Sensorless vector control is an instantaneous electromagnetic torque control technique applied to variable speed (AC) motor drives where the costly speed sensor is no longer used. It is characterized by its fast dynamic response and low cost. Sensorless variable speed drives incorporating induction machines immerged as a result of the progress in the field of power electronics and digital signal processing .

REFERENCES

[1] Jisha. L.K, P.Thomas, A Comparative Study on Scalar and Vector Control of Induction Motors, IEEE 2013.

[2] F. Blashke, The Principle of Filed Orientation as applied to the new trans vector closed loop control system for rotating field machine, Siemens Rev, Vol 39,no.5,pp.217-220,May 1992.

[3] S. Preitl and R-E. Precup, An extension of tuning relation after symmetrical optimum method for PI and PID controllers, Automatica 35(1999), pp.1731-1736.

[4] D.seyoum, the dynamic analysis and control of a self-excited induction generator drivenby a wind turbine, School of Electrical Engineering and Telecommunications March, 2003.

[5] Texas Instruments. TMS320x280x, 2801x, 2804x enhanced quadrature encoder pulse (eqep) module. Texas Instruments, Tech. Rep., December 2008.

APPENDIX A

Table A.1: The parameters of the induction motor for Matlab/Simulink simulation and DSP control implementation

Variable	value
Sn	50*746 (VA)
Un	460 (Vrms)
Rs	0.087 (ohm)
Rr	0.228 (ohm)
Ls=Lr	0. 8 (mH)
Lm	34.7 (mH)
P	2
f	50 (Hz)
J	1.662 (kg.m^2)
fs	10 (KHz)

Table A.2: The calculated Kp and Ki values

	Kp	Ki
Current controller (i)	2.69732	148.34534
Speed controller (ω)	166.2	27700